Theoretical Study on the Reaction of Ground State Cyano Radical with Propylene in Titan's Atmosphere†

C. H. Huang,‡ R. I. Kaiser,§ and A. H. H. Chang*,‡

Department of Chemistry, National Dong Hwa University, Shoufeng, Hualien 974, Taiwan, and Department of Chemistry, University of Hawaii at Manoa, Honolulu, Hawaii 96822

Received: May 30, 2009; Revised Manuscript Received: August 15, 2009

The bimolecular reaction of ground state cyano radical with propylene under the condition of single collision is investigated by combining ab initio electronic structure calculations for predicting reaction paths and RRKM theory to yield rate constant for each path. The isomerization and dissociation channels for each of the seven collision complexes are characterized by utilizing the unrestricted B3LYP/cc-pVTZ level of theory and the CCSD(T)/cc-pVTZ calculations. Sifting with the facilitation of RRKM rate constants through web of ab initio paths composed of 8 collision complexes, 37 intermediates, and 12 H-, 23 H_2-, 3 HCN-, and 4 CH_3-dissociated products, we identify the most probable paths down to 7−9 species at collisions energies of 0 and 5 kcal/mol as the reaction mechanisms. The rate equations of the reaction mechanisms are solved numerically such that the concentration evolutions for all species involved are obtained. This study predicts that CN + $C_2H_3CH_3$ reaction via any of the seven collision complex, **c1**−**c5**, **c7**, and **c8**, would produce **p1**($CH_3CHCHCN$) + H, **p2**(CH_2CHCH_2CN) + H, and mostly **p43**(vinyl cyanide) + CH_3 for collision energy within 0−5 kcal/mol. In addition to the insertion mechanism through collision complex, the direct H-abstraction of propylene by CN radical might occur. Our investigation indicates that the barrierless and exoergic $CN(X^2\Sigma^+)$ + $C_2H_3CH_3(X^1A')$ reaction would be an efficient route for the **p1**, **p2**, and **p43**, and likely HCN formation in cold molecular clouds and in the atmosphere of Saturn's satellite Titan.

I. Introduction

For the last two decades, the atmospheric composition and chemical processing of Saturn's largest satellite, Titan, has been a topic of substantial research from both the astronomical and chemical viewpoints.[1] Today, it is well established that Titan's chemical inventory is the result of a rich photochemistry initiated by photodissociation and electron-impact induced dissociation of molecular nitrogen (N_2; 95−98%) and methane (CH_4; 2−5%), the two main atmospheric constituents. The Voyager I and II spacecrafts[2] together with the Cassini−Huygens mission[3] revealed the presence multiple stratospheric trace constituents. These species can be classified into three groups: hydrocarbon molecules acetylene (C_2H_2), ethylene (C_2H_4), ethane (C_2H_6), methylacetylene (CH_3CCH), propane (C_3H_8), diacetylene (C_4H_2), and benzene (C_6H_6),[4] nitriles like hydrogen cyanide (HCN), cyanoacetylene (HCCCN), and cyanogen (C_2N_2), and finally the oxygen-bearing molecules carbon dioxide (CO_2), carbon monoxide (CO), and water (H_2O). Among them, the nitriles are of particular importance since they are considered as *key intermediates* to form not only astrobiologically relevant molecules but also crucial building blocks of Titan's organic aerosol-based haze layers.[5−15]

The chemical dynamics of photolytically generated, ground state cyano radicals, $CN(X^2\Sigma^+)$, with unsaturated hydrocarbons are of paramount importance in understanding the formation of these nitrile molecules such as cyano acetylene (HCCCN).[16,17] However, although the main source of the cyano radicals has been characterized as the photolysis of hydrogen cyanide (HCN),[18−23] the underlying chemical dynamics and kinetics of bimolecular cyano radical reactions and the role in the buildup of complex hydrocarbons have started to emerge only recently.[24] Laboratory studies of cyano radical reactions with unsaturated hydrocarbons utilizing the crossed molecular beams method

TABLE 1: Product Branching Ratios at Collision Energy of Zero and 5 kcal/mol for the Reactions CN + $C_2H_3CH_3$, CN + CD_3CHCH_2, and CN + CH_3CDCD_2, Obtained for the Reaction Mechanisms Shown in Figures 9, s8 (Supporting Information), and s10 (Supporting Information), Respectively

mechanism	collision energy			
CN + $C_2H_3CH_3$		**p1** + H	**p2** + H	**p43** + CH_3
c1	0	0.12	0.18	0.70
	5 kcal/mol	0.16	0.26	0.57
c3	0	0.06	0.08	0.86
	5 kcal/mol	0.06	0.09	0.85
c5	0	0.09	0.13	0.77
	5 kcal/mol	0.12	0.19	0.70
CN + CD_3CHCH_2		**p1** + H	**p2** + D	**p43** + CD_3
c1	0	0.12	0.06	0.82
	5 kcal/mol	0.17	0.12	0.71
c3	0	0.06	0.03	0.90
	5 kcal/mol	0.07	0.05	0.88
c5	0	0.09	0.05	0.86
	5 kcal/mol	0.13	0.09	0.79
CN + CH_3CDCD_2		**p1** + D	**p2** + H	**p43** + CH_3
c1	0	0.05	0.16	0.79
	5 kcal/mol	0.08	0.26	0.66
c3	0	0.02	0.08	0.89
	5 kcal/mol	0.03	0.10	0.87
c5	0	0.04	0.13	0.84
	5 kcal/mol	0.06	0.19	0.75

† Part of the "Russell M. Pitzer Festschrift".

* Corresponding author. E-mail: hhchang@mail.ndhu.edu.tw. Fax: +886-3-8633570.

‡ National Dong Hwa University.

§ University of Hawaii at Manoa.

10.1021/jp905081u CCC: $40.75
Published on Web 09/22/2009

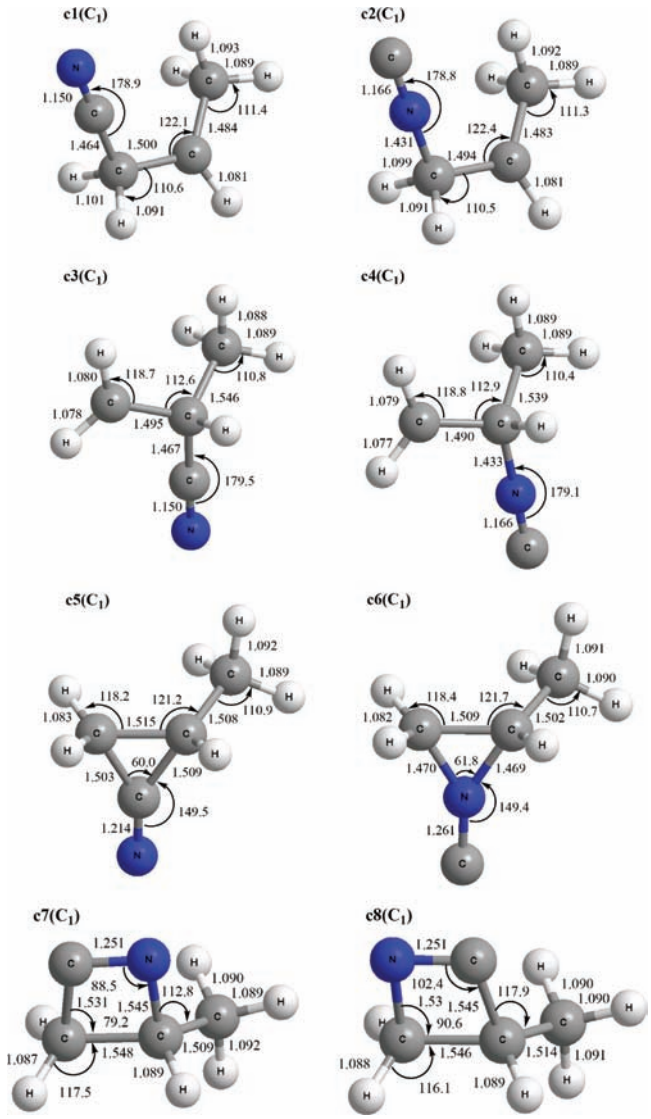

Figure 1. B3LYP/cc-pVTZ optimized geometries of the eight collision complexes of the $CN(^2\Sigma^+) + C_2H_3CH_3(^1A')$ reaction, in which the point group is in parentheses, lengths in angstrom, and the angles in degree.

provided valuable input data into chemical models of Titan demonstrating the potential of this approach. These were the formation of cyano acetylene (HCCCN), vinyl cyanide (C_2H_3CN), cyanobenzene (C_6H_5CN), 1-cyanoallene ($H_2CCCHCN$), and 1- and 3-cyanomethylacetylene (CH_3CCCN; $HCCCH_2CN$), as well as 3-butenenitrile (H_2CCDCD_2CN) and cis/trans 2-butenenitrile ($CD_3CHCHCN$) plus atomic hydrogen from reactions of cyano radicals with acetylene,[25] ethylene,[26] benzene,[27] allene,[28] methylacetylene,[29] and propylene,[30] respectively. Recent kinetics experiments at temperatures as low as 13 K demonstrated nicely that cyano radical reactions with unsaturated hydrocarbons are indeed very fast at a level of a few 10^{-10} cm^3s^{-1} and proceeded without entrance barriers.[31] However, these experiments monitored only the decay kinetics of the cyano radical, and reaction products could not be sampled. On the other hand, crossed molecular beam experiments can hardly provide temperature dependent rate constants and might have difficulties under some circumstances to identify kinetically less favorable channels. Therefore, a combination of kinetics experiments with crossed molecular beams data and electronic structure calculations supply a unique approach to elucidate the open channels and the underlying branching ratios if multiple channels are involved. In an ongoing interest to elucidate the reaction mechanisms of ground state cyano radicals with unsaturated hydrocarbons, we present here a combined electronic structure and RRKM treatment of this system. Recently, crossed beams studies,[30] kinetic investigations,[32] electronic structure calculations,[33] and photoionization of this reaction utilizing the Advanced Light Source[34] have been carried out.

In this work, our aim is to first identify through ab initio calculations the exoergic channels without entrance barrier, which would be competitive kinetically, second, to derive the reaction mechanism by computing the RRKM rate constants of elementary steps specifically tuned for the condition of single binary-collision, subsequently, to obtain concentration evolutions for the species involved by solving the rate equations for the reaction mechanism, and finally, to predict the product yields at different collision energies.

II. Theoretical Methods

1. Ab Initio Reaction Paths Prediction. With the assumption that the $CN(^2\Sigma^+) + C_2H_3CH_3(^1A')$ reaction proceeds on the adiabatic doublet ground state potential energy surface of C_4H_6N, the pathways under single collision are inferred theoretically. Possible collision complexes are identified, followed by the characterization of low-energy isomerization channels for each collision complex. The optimized geometries and harmonic frequencies of intermediates, transition states, and dissociation products are obtained at the level of the hybrid density functional theory, the unrestricted B3LYP[35]/cc-pVTZ, with energies refined by the coupled cluster[36] CCSD(T)/cc-pVTZ with unrestricted B3LYP/cc-pVTZ zero-point energy corrections. It was demonstrated previously[37] that when the basis functions of 6-311G(d,p) and 6-311+G(3df,2p) are employed for B3LYP and CCSD(T), respectively, the energies obtained by this procedure are in agreement with experimental values within 1−2 kcal/mol. The GAUSSIAN98 and 03 programs[38] are employed in the electronic structure calculations.

2. RRKM Rate Constant Calculations. Assuming that the reaction rate could be described statistically, namely, the energy is equilibrated among molecular degrees of freedom before the reaction occurs, and provided the energy is conserved such as in molecular beam experiments where the condition for single collision is warranted, the rate constant could be predicted by RRKM theory. That is, for a reaction

$$A^* \xrightarrow{k} A^{\ddagger} \rightarrow P$$

where A* is the energized reactant, $A^{\ddagger}$ represents the transition state, and P the products, the rate constant $k(E)$ may be expressed as

$$k(E) = \frac{\sigma}{h}\frac{W^{\ddagger}(E - E^{\ddagger})}{\rho(E)} \quad (1)$$

where σ is the symmetry factor, $W^{\ddagger}$ is the number of states of the transition state, $E^{\ddagger}$ is the transition state energy, and ρ is the density of states of the reactant. In this work, ρ and $W^{\ddagger}$ are computed by saddle-point method,[39,40] molecules are treated as collections of harmonic oscillators whose harmonic frequencies are obtained as described in section II.1. The rate constants are computed at nine collision energies, 0.0, 0.03, 0.15, 0.27, 0.48, 0.9, 2.0, 5, and 10 kcal/mol, which correspond to average kinetic

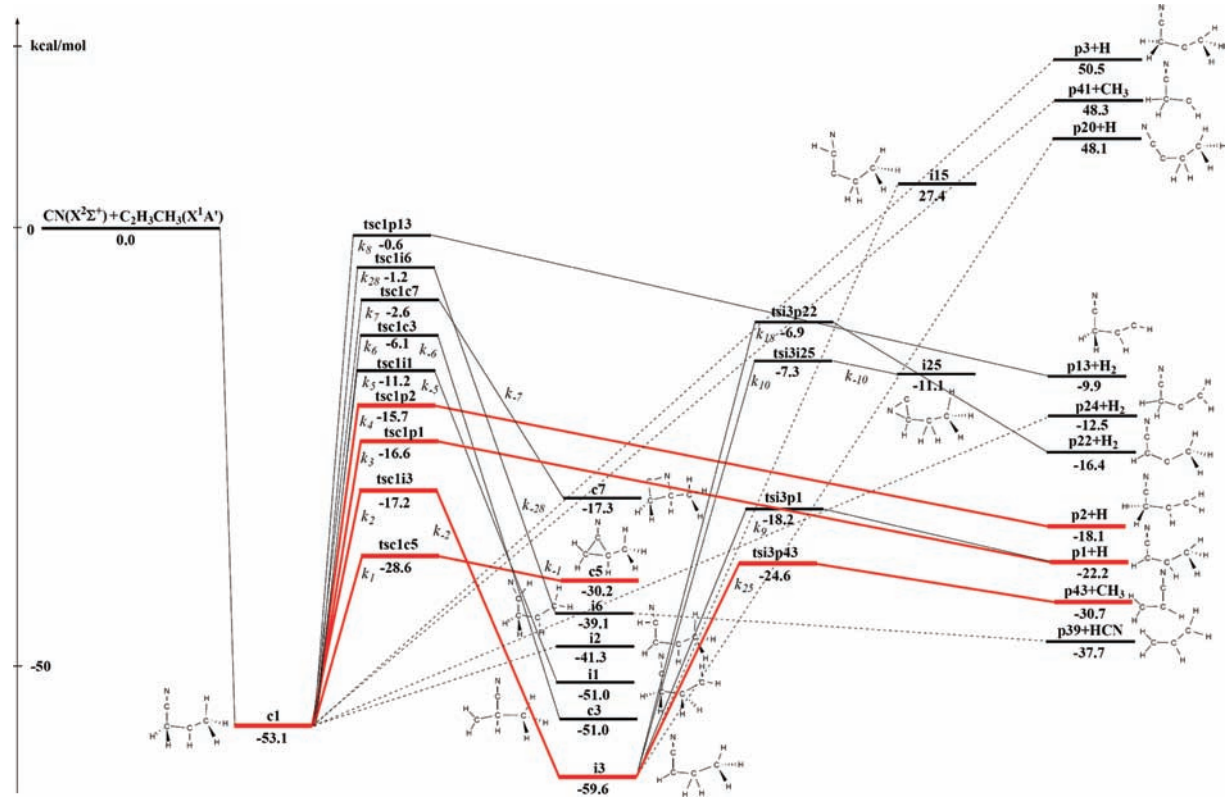

Figure 2. Reaction paths and the most probable paths (highlighted) at zero collision energy of the collision complex, **c1**, in which the energies are computed at CCSD(T)/cc-pVTZ level of theory with B3LYP/cc-pVTZ zero-point energy corrections at the B3LYP/cc-pVTZ optimized geometries. Note for those paths in dotted lines, the attempts are not made or not successful in locating the transition states.

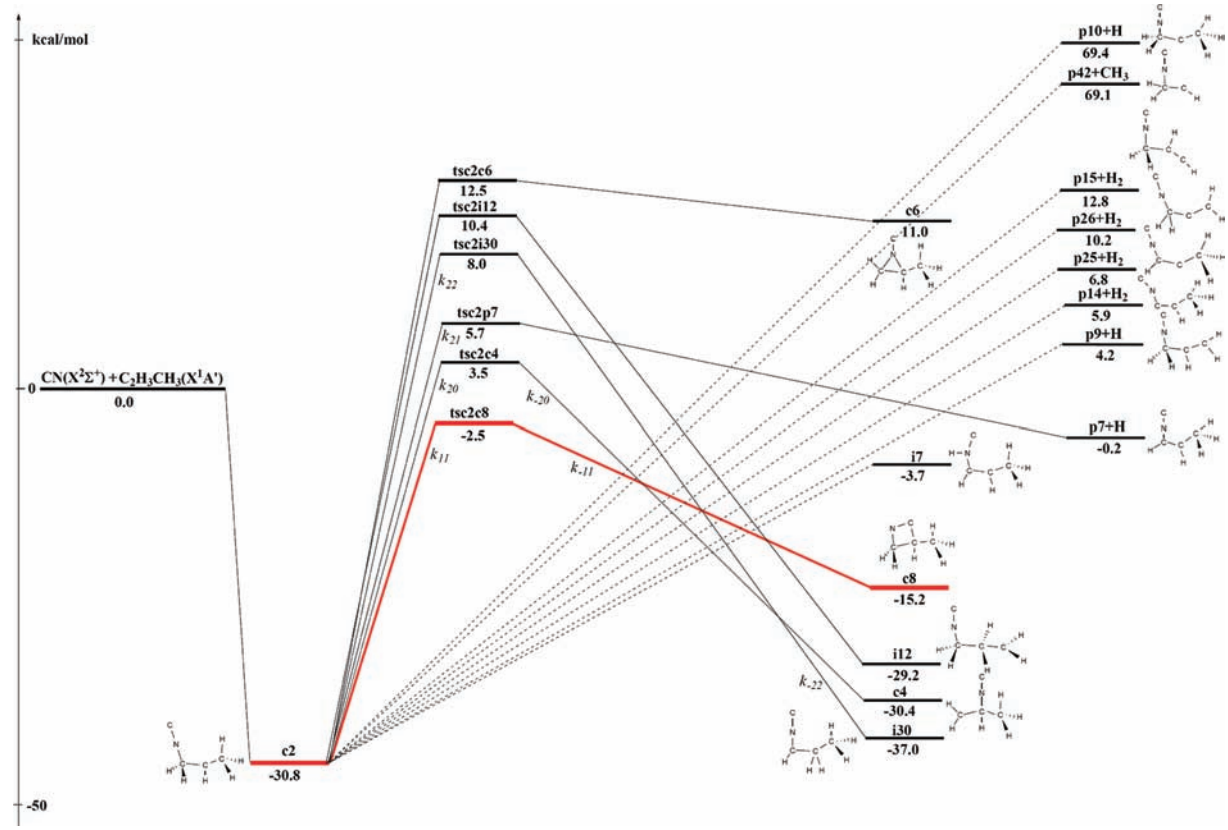

Figure 3. Reaction paths and the most probable paths (highlighted) at zero collision energy of the collision complex, **c2**, in which the energies are computed at CCSD(T)/cc-pVTZ level of theory with B3LYP/cc-pVTZ zero-point energy corrections at the B3LYP/cc-pVTZ optimized geometries. Note for those paths in dotted lines, the attempts are not made or not successful in locating the transition states.

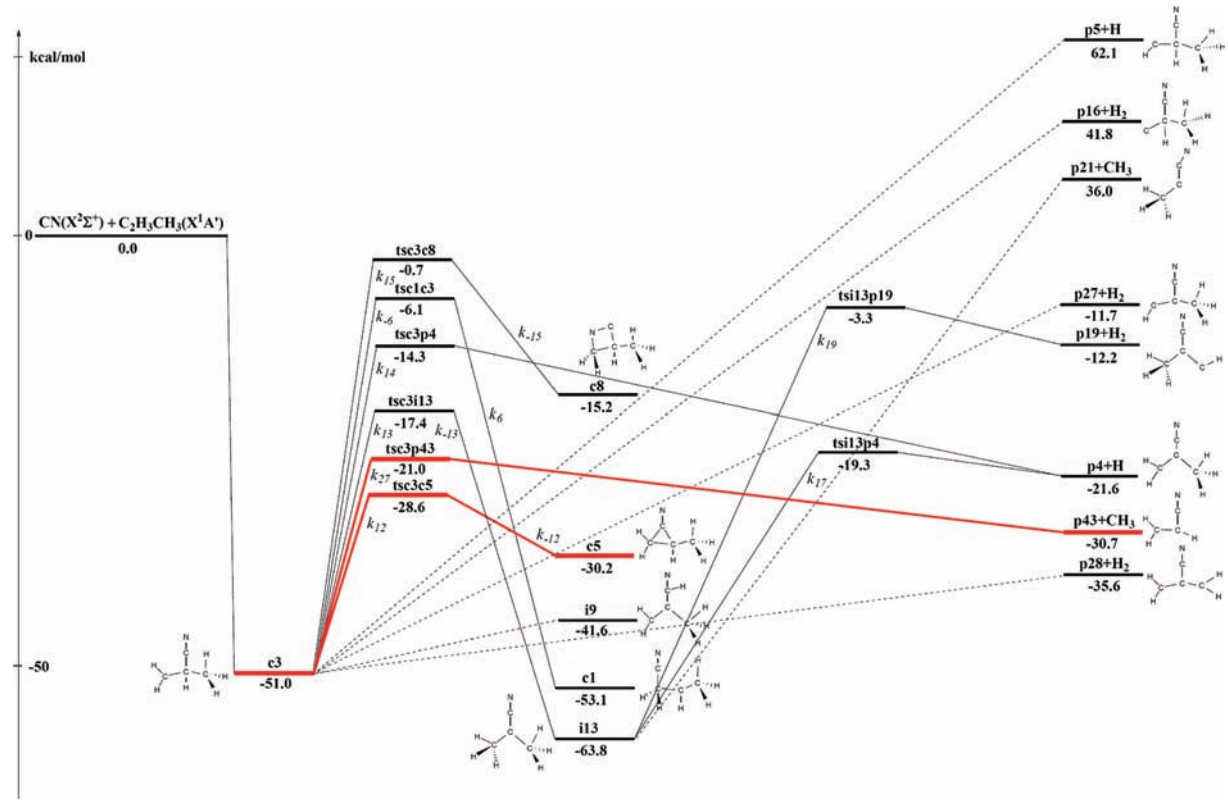

Figure 4. Reaction paths and the most probable paths (highlighted) at zero collision energy of the collision complex, **c3**, in which the energies are computed at CCSD(T)/cc-pVTZ level of theory with B3LYP/cc-pVTZ zero-point energy corrections at the B3LYP/cc-pVTZ optimized geometries. Note for those paths in dotted lines, the attempts are not made or not successful in locating the transition states.

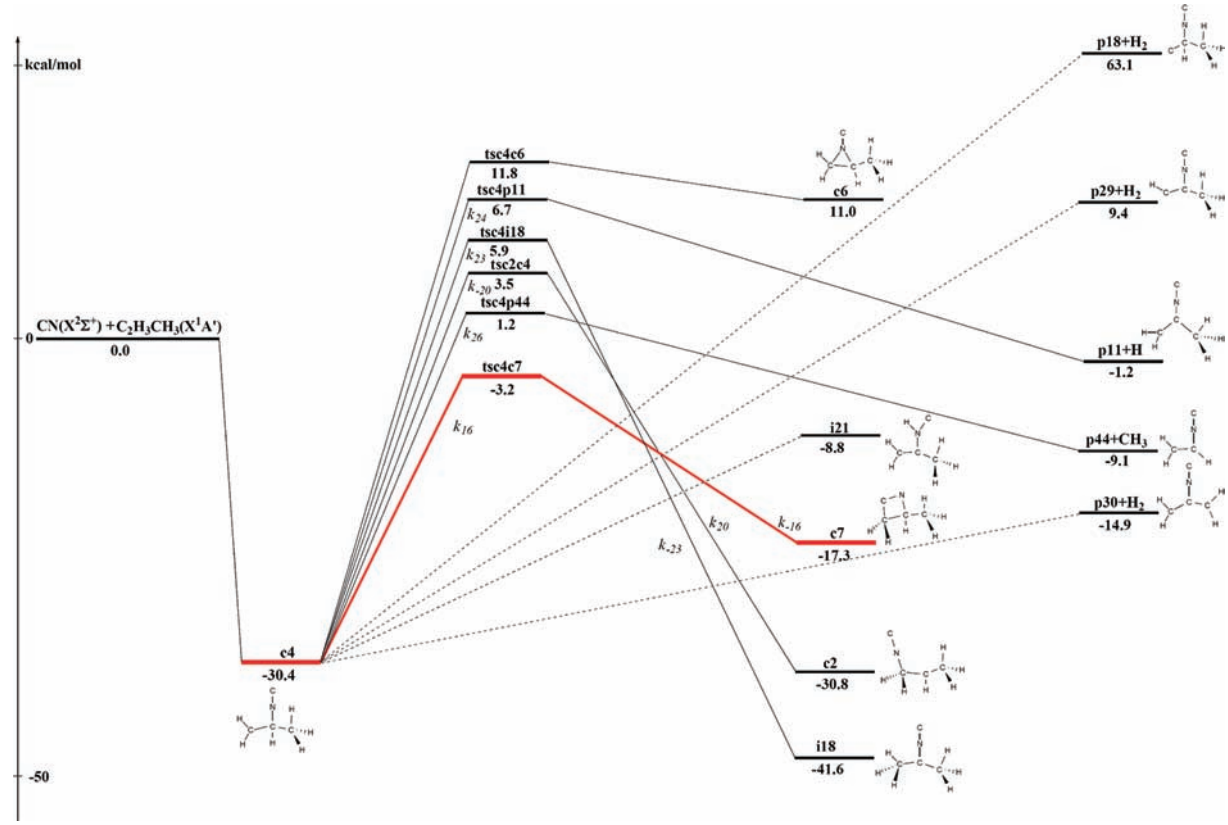

Figure 5. Reaction paths and the most probable paths (highlighted) at zero collision energy of the collision complex, **c4**, in which the energies are computed at CCSD(T)/cc-pVTZ level of theory with B3LYP/cc-pVTZ zero-point energy corrections at the B3LYP/cc-pVTZ optimized geometries. Note for those paths in dotted lines, the attempts are not made or not successful in locating the transition states.

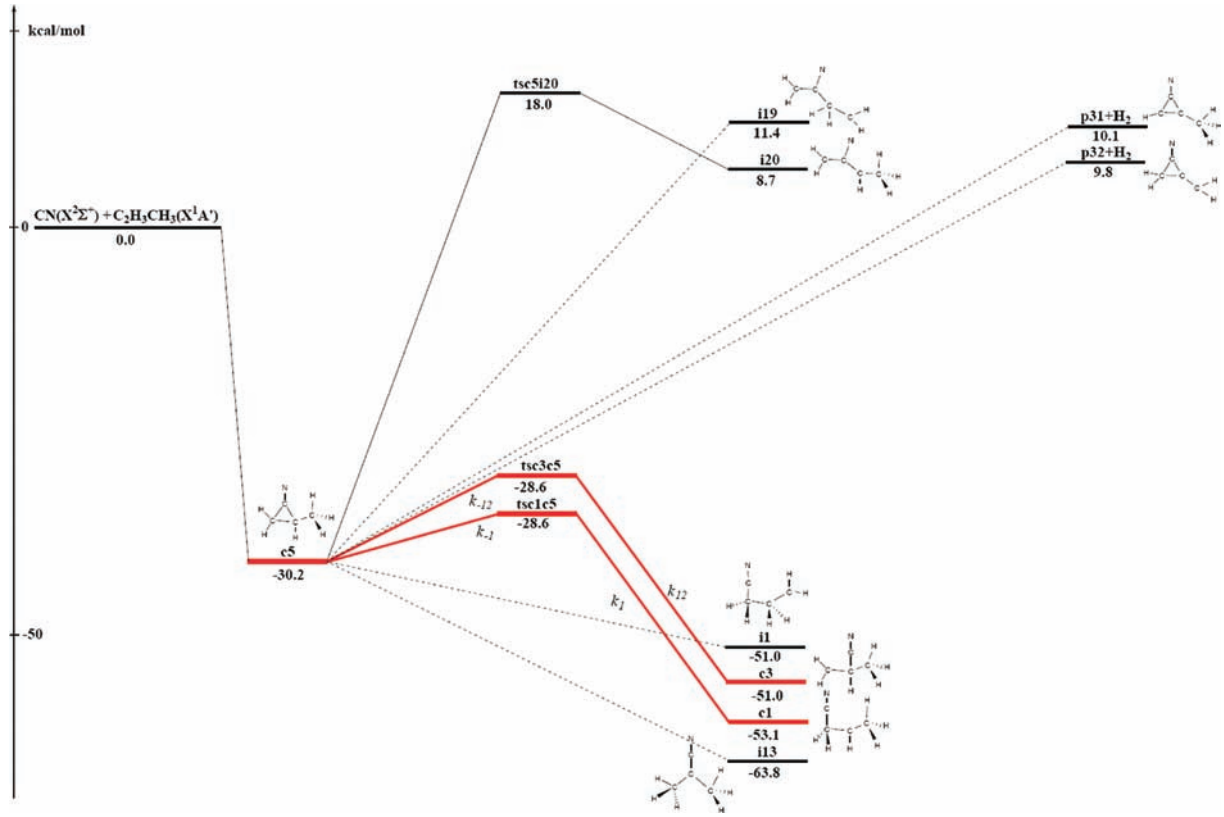

Figure 6. Reaction paths and the most probable paths (highlighted) at zero collision energy of the collision complex, **c5**, in which the energies are computed at CCSD(T)/cc-pVTZ level of theory with B3LYP/cc-pVTZ zero-point energy corrections at the B3LYP/cc-pVTZ optimized geometries. Note for those paths in dotted lines, the attempts are not made or not successful in locating the transition states.

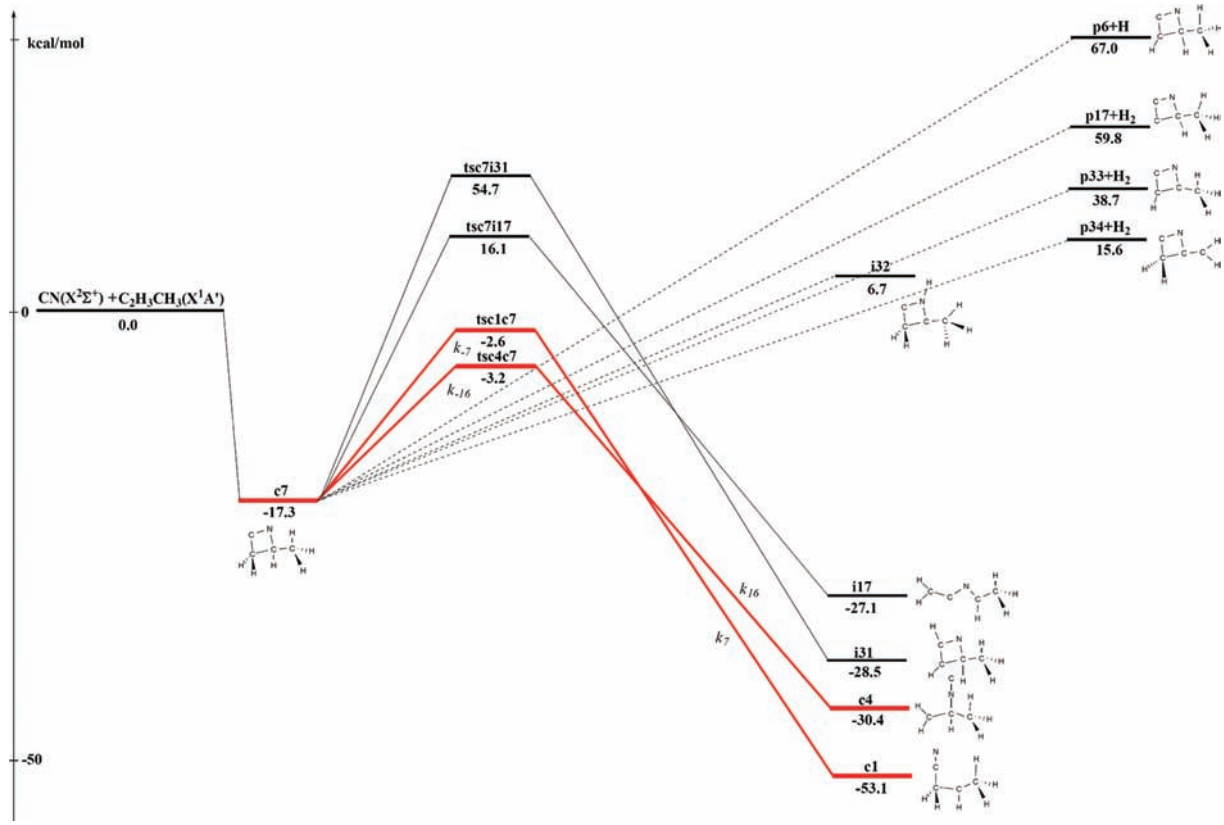

Figure 7. Reaction paths and the most probable paths (highlighted) at zero collision energy of the collision complex, **c7**, in which the energies are computed at CCSD(T)/cc-pVTZ level of theory with B3LYP/cc-pVTZ zero-point energy corrections at the B3LYP/cc-pVTZ optimized geometries. Note for those paths in dotted lines, the attempts are not made or not successful in locating the transition states.

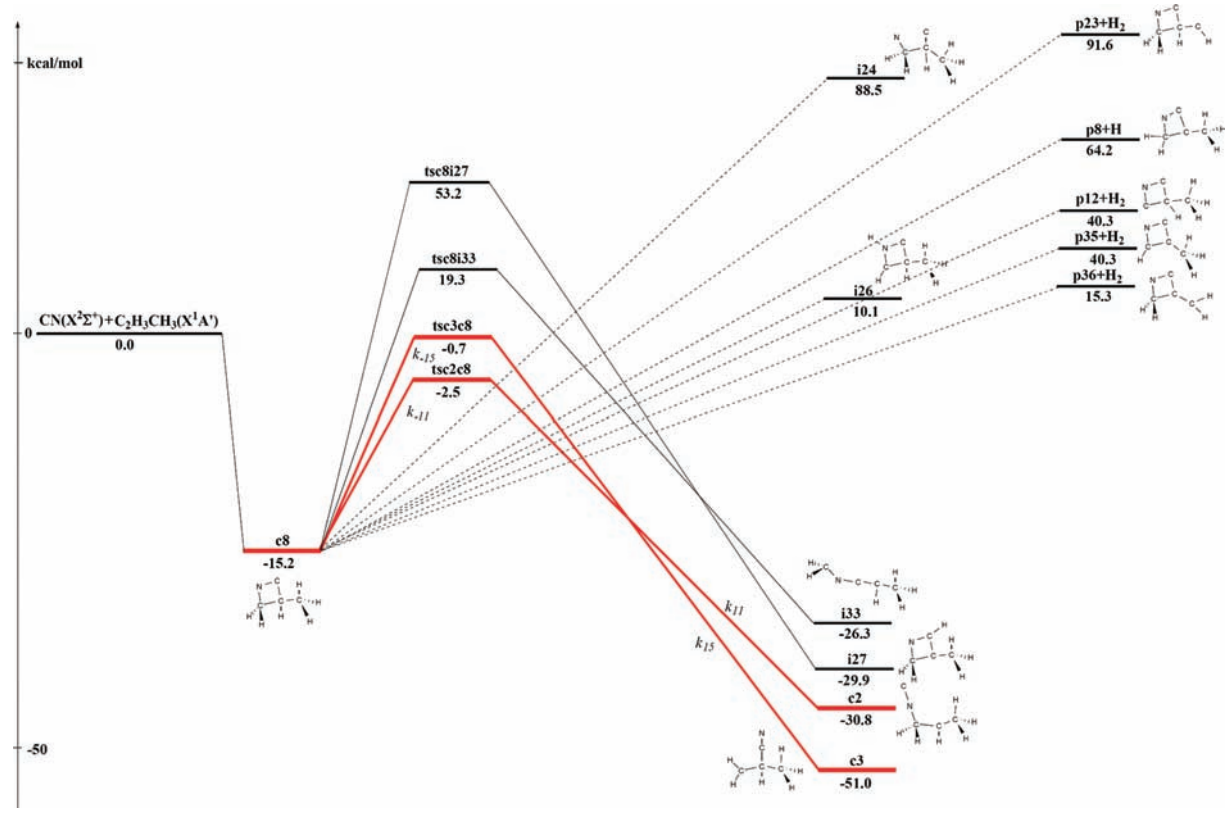

Figure 8. Reaction paths and the most probable paths (highlighted) at zero collision energy of the collision complex, **c8**, in which the energies are computed at CCSD(T)/cc-pVTZ level of theory with B3LYP/cc-pVTZ zero-point energy corrections at the B3LYP/cc-pVTZ optimized geometries. Note for those paths in dotted lines, the attempts are not made or not successful in locating the transition states.

energies of an ideal gas molecule at temperatures of 0, 10, 50, 90, 160, 300, 671, 1678, and 3355 K, respectively.

3. Solution of the Rate Equations: Concentration Evolutions and Branching Ratios. The rate equations for reaction mechanism of each collision complex are solved by the numerical Runge−Kutta method at collision energies of 0 and 5 kcal/mol. The solutions yield the concentrations of species in the reaction mechanisms as a function of time, the concentration evolutions.

III. Results and Discussion

The titled reaction could be initiated by the attack of electrophilic cyano radical to the π system of the propylene molecule. The B3LYP/cc-pVTZ optimized geometries of the eight possible collision complexes as a result of such attack are denoted **c1**−**c8** as illustrated in Figure 1. All of them are found energetically bound relative to the reactants with the exception of **c6**, a three-member ringed isonitrile. The reaction paths of the titled reaction are assembled by tracing the routes for individual collision complex. The immediate channels of **c1**−**c5**, **c7**, and **c8** including low-energy isomerizations of hydrogen shift, CN shift, ring formation, ring-opening, hydrogen atom dissociation, hydrogen molecule and CH_3 elimination are identified; for the pathways with energy under10 kcal/mol (relative to the reactants), the rate constants are then estimated. The computed rate constants facilitate in sifting through the web of reaction channels for the most kinetically competitive so that only the immediate channels for those intermediates produced with the largest rate constants are pursued further until the dissociation is encountered.

The B3LYP/cc-pVTZ optimized structures of intermediates, dissociation products, and transition states, designated as **i**, **p**, and **ts**, are drawn in Figures s1, s2, and s3 (Supporting Information),[41] respectively; their predicted energies are listed in Table s1 (Supporting Information)[41] and the rate constants computed at collision energies of 0.0, 0.03, 0.15, 0.27, 0.48, 0.9, 2.0, 5, and 10 kcal/mol in Table s2 (Supporting Information).[41] The CCSD(T)/cc-pVTZ energetic paths of **c1**−**c5**, **c7**, and **c8** are plotted in Figures 2−8, respectively. In the discussion that follows, the energies cited are the CCSD(T)/cc-pVTZ energies relative to the reactants with B3LYP/cc-pVTZ zero-point energy corrections, and the quoted rate constants are computed at zero collision energy if not otherwise stated.

1. Dissociation Products. Among the twelve relevant H-dissociation products, **p1**, **p2**,**p4**, **p7**, and **p11** are of energies lower than the reactants as listed in Table s1 (Supporting Information) and their geometries displayed in Figure s2 (Supporting Information). As many as seven H_2-dissociation products are predicted of lower energies or more stable than the reactants out of relevant twenty-three. Three distinct products (**p37**, **p39**, **p40**) of H abstraction by CN from propylene are all bound. As a result of dissociating CH_3, **p43** (vinyl cyanide) and **p44** are more stable than the reactants, while **p21**, **p41** and **p42** are much higher in energy. However, as rationed in the sections that follow, only **p43**, **p1**, and **p2**, and likely, **p39** and **p40** remain significant; despite being energetically accessible, the rest are edged out kinetically.

2. Reaction Paths and the Most Probable Paths. ***c1 Paths.*** As seen in Figure 2, ten low-energy channels are characterized for **c1**: ring closures to fellow collision complexes **c5** and **c7**, 1,2 H-shifts to **i1** and **i3**, H-shift to **i6**, CN-shift to **c3**, H-losses to generate **p1** and **p2**, H_2 elimination to **p13**, and CN dissociation back to the reactants. The transition state for the H-shifting to **i2** could not be located, and likewise, the transition

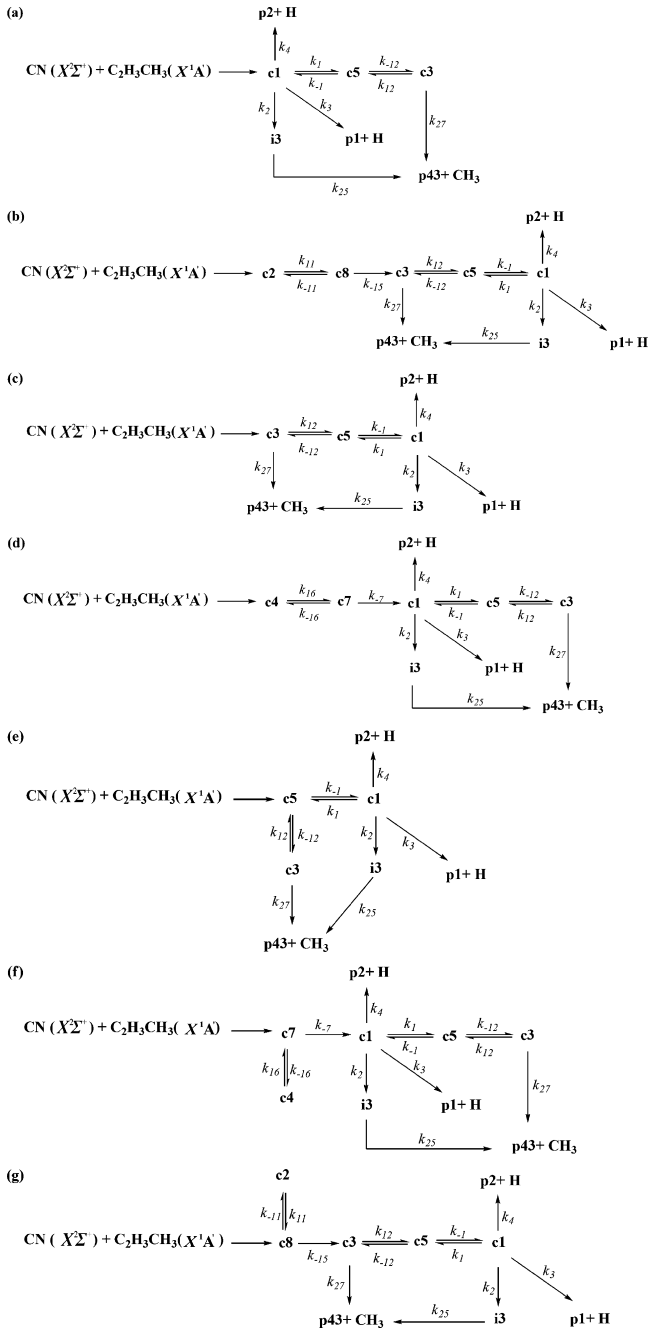

Figure 9. Reaction mechanisms (**a**)−(**g**) derived from the most probable paths at zero and 5 kcal/mol collision energy of collision complexes **c1**−**c5**, **c7**, and **c8**, respectively, in which the k's are the corresponding rate constants.

state for producing **p24** + H_2. The minimum energy path **c1** → **c5** is indeed the kinetically most competitive as confirmed by the RRKM predicted corresponding rate constant k_1. As discussed later, **c5** would turn back to **c1**. Thus **c1** should look for the next likely pathways to release its concentration buildup, which include **c1** → **i3**, **c1** → **p1** + H, and **c1** → **p2** + H with comparable rate constants, k_2 ($7.97 \times 10^6 s^{-1}$), k_3 ($1.42 \times 10^7 s^{-1}$), and k_4 ($2.07 \times 10^7 s^{-1}$), respectively. At low energy, **i3** could break a CH_3 radical to form **p43**, isomerize back to **c1**, dissociate a hydrogen atom to **p1**, eliminate a H_2 to become **p22**, or form a three-member ringed **i25**; it turns out that the rate constant k_{25} (**i3** → **p43** + CH_3) is leading the rest by at least 50 times.

c2 Paths. The only accessible pathway for **c2** at zero collision energy is the ring closing to **c8**, as seen in Figure 3.

c3 Paths. The three-member ring formation and CH_3 dissociation that yield **c5** and **p43**, respectively, would be the swiftest by a significant margin among the six bound channels which include H-shift to **i13**, a direct CN-shift to **c1**, four-member ring closure to **c8**, and H-dissociation to **p4**. The transition states for hydrogen-shift to generate **i9**, H_2-loss to **p28** and **p27** could not be located.

c4 Paths. Rather similar to that for **c2**, the ring-closure to become **c7** is the only channel that is all the way bound.

c5 Paths. **c5** could easily open its three-member ring and convert to the two most stable collision complexes **c1** and **c3** with comparable rate constants while the third possible isomer **i20** is at much higher 8.7 kcal/mol. The transition states for H-shift accompanied by ring-breaking to produce **i1** and **i13** are not found.

c7 Paths. Ring-opening could bring **c7** to **c4** and **c1** with an almost 2:1 ratio as revealed by the rate constants at zero collision energy.

c8 Paths. Similar to **c7**, **c8** is able to open its four-member ring and arrives at **c2** and **c3** without additional collision energy. The ring-openings to **i33** and **i24** are difficult to achieve due to the much higher energies of 19.3 and 88.5 kcal/mol for the **tsc8i33** and **i24**, respectively. Seemingly, the corresponding rate constants indicate that the **c8** → **c2** reaction is 24 times more efficient than the **c8** → **c3**; however, the sole choice for **c2** would be returning to **c8**, which in turn puts **c8** eventually proceeding via the channels of **c3**.

3. Reaction Mechanism. The most probable paths of **c1**−**c5, c7,** and **c8** highlighted in Figures 2−8, respectively, are determined on the basis of the kinetic competitiveness at zero collision energy, meaning the paths with leading rate constants but not necessarily the minimum energy paths. The same paths persist as the collision energy rises to 5 kcal/mol. The reaction mechanisms according to the most probable paths are presented in Figure 9, which clarifies the directions of reaction. It demonstrates clearly that there are three likely dissociation products, **p43** + CH_3, **p1** + H, and **p2** + H, and that the collision complexes isomerize among themselves, namely, **c3**, a nitrile, would shift CN by way of the CNC ringed **c5** and convert to the most stable nitrile **c1** while the iso-nitriles **c2** and **c4** initially form the CCCN ringed **c8** and **c7**, respectively, and subsequently likewise arrive at **c1**. By way of **c1**, all seven collision complexes eventually dissociate a hydrogen atom of the CH_2 or CH_3 group to yield **p1** or **p2**, respectively, and via both **c1** (thus **i3**) and **c3,** generate the major product, **p43** + CH_3.

4. Concentration Evolutions. The rate equations for mechanisms of CN + $C_2H_3CH_3$ reaction proceeding via collision complexes **c1**−**c5**, **c7**, and **c8** as given in Figure 9a−g are solved numerically with employment of the RRKM rate constants in Table s2 (Supporting Information) for these seven sets of simultaneous differential equations in 7, 9, 7, 9, 7, 9, and 9 unknown concentrations, respectively. The solutions, concentration evolutions with time, thus obtained at zero and 5 kcal/mol collision energies for species in **c1** mechanism are laid out in Figure 10, and those for **c2**−**c5**, **c7**, and **c8** are in Figures s4 and s5 (Supporting Information).[41]

Figure 10 indicates when the titled reaction proceeds via collision complex **c1**, **c1** dies down and the dissociation products **p1** and **p2** rise up in 10^{-8} s as limited by the bottleneck rate constant, k_2 ($7.97 \times 10^6 s^{-1}$) at zero collision energy. During the reaction, the intermediates, **c5** and **i3,** peak around nanoseconds, however, to the negligible 2.06×10^{-5} and 4.87×10^{-3} in concentration, respectively, as **c3** develops to a decent

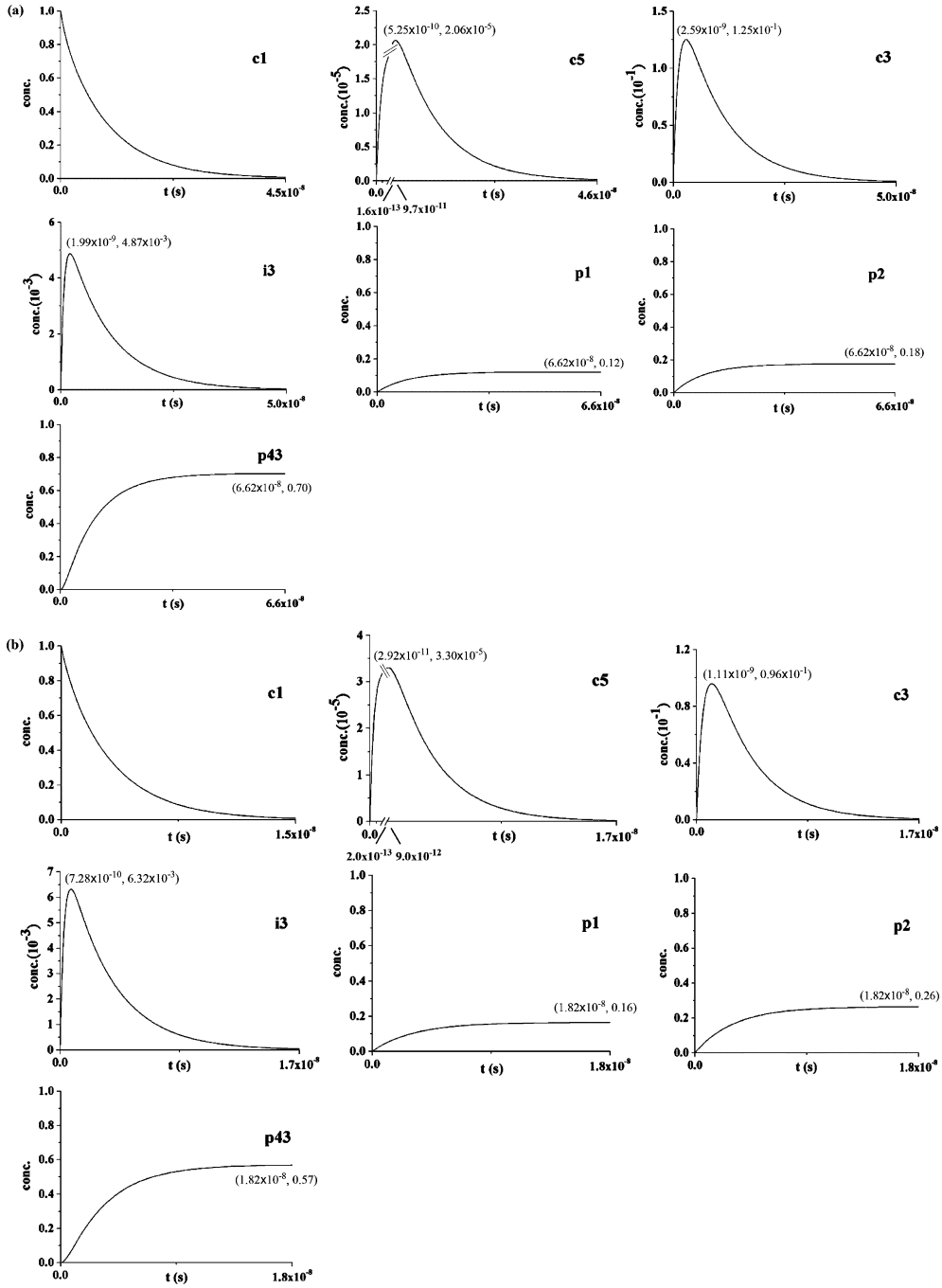

Figure 10. (a) Concentration evolution for each species in **c1** reaction mechanism at zero collision energy as in Figure 9a. (b) Concentration evolution for each species in **c1** reaction mechanism at 5 kcal/mol collision energy as in Figure 9a.

0.13. The yield of **p43**:**p2**:**p1** is 0.70:0.18:0.12. As the collision energy elevates to 5 kcal/mol, the trend sustains with earlier peaks and completion due to generally larger rate constants; the ratio for **p43**:**p2**:**p1** becomes 0.57:0.26:0.16. **p43** + CH_3 is firmly the major product even though higher collision energy gives advantage to the H-dissociated products, **p1** and **p2**.

At collision energy of zero and 5 kcal/mol, the branching ratio of **p1** and **p2** would be in fact exactly the same for the CN + $C_2H_3CH_3$ proceeding via the paths of any of **c1**−**c5**, **c7**, and **c8**, since it is solely determined by the common **c1** routes. Since **p43** is generated by both **c1** (via **i3**) and **c3**, its final yield would depend on the concentrations of **c1** and **c3**. Thus for the titled reaction assuming the mechanism of **c1**, **c4**, and **c7**, which corresponds to the (a), (d), and (f), the **p43** yield is the same 0.7 and 0.57 at zero and 5 kcal/mol, respectively, as indicated in Figure 10. Likewise, **c2** and **c8** take the same sequence as **c3** before reaching **p43**, which results in the three eventually share the same **p43** yield of 0.86 and 0.85 at zero and 5 kcal/mol collision energy, respectively, as shown in Figures s4 and s5 (Supporting Information). By the same argument, it is not surprising that **c5** evolves to a unique **p43** yield.

5. Comparison with Previous Works. ***Previous Works.*** Utilizing deuterated isotopologues of propylene, CD_3CHCH_2 and CH_3CDCD_2, Gu et al.[30] were able to confirm by crossed beam experiments that the hydrogen atom can be eliminated from the vinyl and methyl groups of collision complex **c1** to form **p1** and **p2**, respectively. With photoionization mass spectrometry, Trevitt et al.[34] identified multiple products for CN + propylene reaction at room temperature (4 Torr), in which 75% are **p43** from CH_3 elimination channel, and 25% hydrogen atom

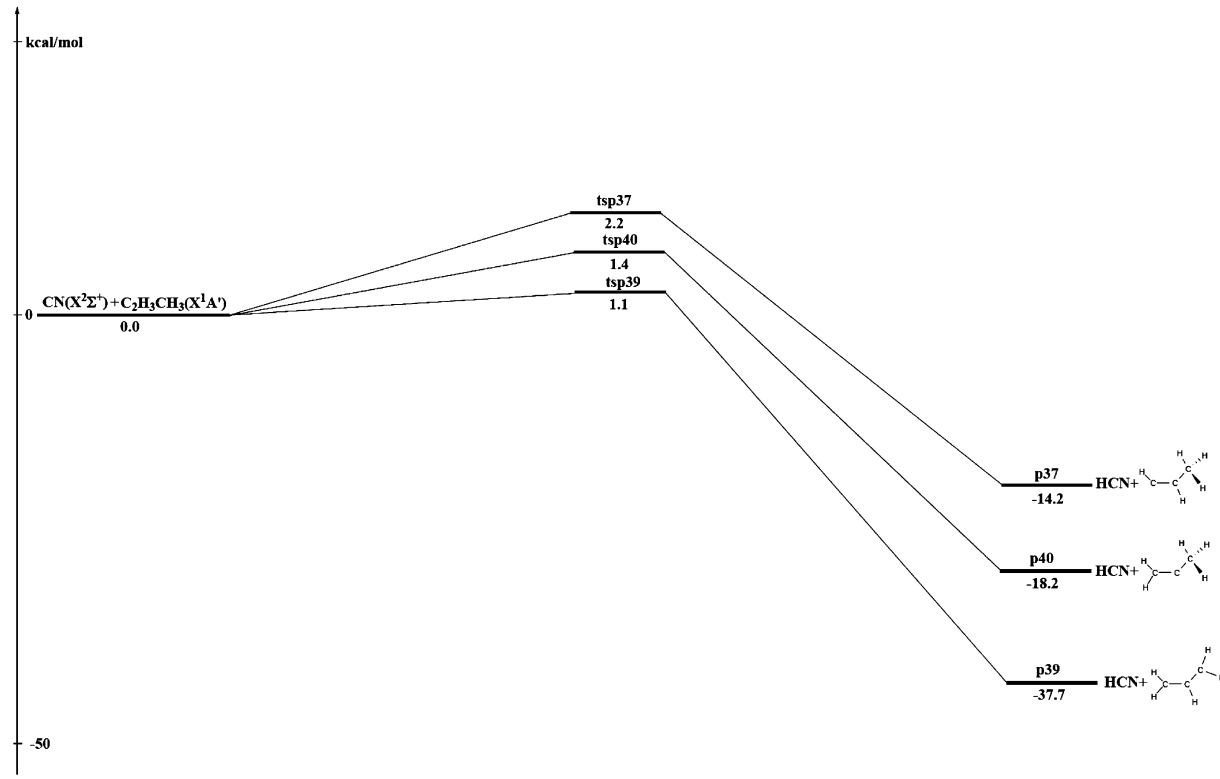

Figure 11. Paths of hydrogen-abstraction by CN, in which the energies are computed at CCSD(T)/cc-pVTZ level of theory with B3LYP/cc-pVTZ zero-point energy corrections at the B3LYP/cc-pVTZ optimized geometries.

elimination. Among the products determined for H elimination, 57% are **p1** and 43% **p4**; **p2** is not detected but is estimated to be no more than 15%; no evidence of HCN was found. The experiments performed by Gu et al. could not distinguish between **p1** and **p4**, both of which could be the products of hydrogen atom ejection from the vinyl group of **c1**; however, the formation of **p2** is certain. By monitoring CN decay and H atom growth by laser-induced fluorescence, Gannon et al.[33] reported pressure dependent H atom yields of 0.478 (±0.045) ~ 0.003(±0.006) in the range of 2−200 Torr at room temperature for the titled reaction. Since only H atoms among various products were detected in this work, the reaction paths that lead to **p1** + H, **p4** + H, **p43** + CH_3, and **p39** + HCN were obtained by ab initio G3X calculations, and subsequently were employed in the master-equation calculation to facilitate in predicting the branching ratios. Though detected in both crossed beams experiments[30] and photoionization study,[34] **p2** was not considered in the investigation of Gannon et al.[33] Their results indicated that the HCN production was very minor as also concluded in the RRKM-master equation analysis of CN + ethylene by Vereecken et al.[42]

Implications of the Present Work. Consistent with the findings of Gannon et al. and Trevitt et al., our investigation confirms that at zero pressure the major channel is the CH_3 dissociation via **c3** and **i3** to generate **p43**, and that H atom elimination is an important pathway. The present work also lends support to the detection of **p1** and **p2** in the crossed beam experiments.[30]

As seen in Figure 4, the formation of **p4** can be achieved even at zero collision energy through either one-step H atom dissociation from **c3** with the **tsc3p4** at −14 kcal/mol or, sequentially, **c3** → **i13** → **p4** + H. Thus the observation of **p4** in the photoionization study by Trevitt et al. is reasonable, considering that the **p4** production is quite energetically feasible. Due to the kinetic concerns, **p4** paths are not included in the reaction mechanisms deduced in Figure 9. To estimate **p4** branching ratio under zero pressure or collision free condition such as in the crossed beam experiments of Gu et al. carried out at collision energy close to 6 kcal/mol, expanded mechanisms of **c1**, **c3**, and **c5** that incorporate **p4** are derived as in Figure s6 (Supporting Information).[41] At collision energy of 5 kcal/mol, by solving the corresponding rate equations for Figure s6 the branching ratios of **p43**:**p1**:**p2**:**p4** are predicted to be 0.56:0.16:0.26:0.02 via **c1** mechanism, 0.82:0.06:0.09:0.03 via **c3**'s, and 0.68:0.12:0.19:0.02 if through **c5**'s.

The reactions of CN radical with the deuterated isotopologues, CD_3CHCH_2 and CH_3CDCD_2, are examined to give insights into the crossed beam experiments.[30] The reaction paths and mechanisms via **c1**, **c3**, and **c5** for CN + CD_3CHCH_2 reaction are given in Figures s7 and s8 (Supporting Information),[41] respectively, and for CN + CH_3CDCD_2, Figures s9 and s10 (Supporting Information).[41] The rate constants at zero and 5 kcal/mol collision energy are listed in Table s3 and s4 (Supporting Information),[41] and their product branching ratios are displayed in Table 1 along with those for the reaction of CN + $C_2H_3CH_3$. As clearly seen from Table 1, for the systems of deuterated propylene, the H elimination channel consistently dominates its D elimination counterpart, mainly due to a higher barrier for the latter. As a consequence, the yield of **p1** + H is higher than **p2** + D in CN + CD_3CHCH_2 and for CN + CH_3CDCD_2, **p2** + H is favored over **p1** + D, even though there is more **p2** + H than **p1** + H in the reaction of CN + $C_2H_3CH_3$.

6. H-Abstraction by CN. Due to the three nonequivalent hydrogen groups in propylene, there could be three pathways to produce HCN as a result of direct H-abstraction by CN. The channels of H-abstraction by CN presented in Figure 11 indicate that the products are all bound relative to the reactants as the transition states are of positive energies. It is noted that the transition state for HCN + **p37**($CHCHCH_3$) seems certain while the assignment of the ones for HCN + **p40**(CH_2CCH_3) and HCN

+ **p39**(CH_2CHCH_2) are quite tentative with present level of calculations. Since the structures of these three transition states resemble the reactants rather than the products, particularly HCN, the process would result in vibrationally excited HCN molecules. The difficulty in locating the transition states might imply that the formations of **p39** and **p40** are barrierless and thus highly likely to occur energetically. However, no evidence of HCN formation detected in experiments[34] appears to support all three channels in fact have barriers.

7. Notes on C_4H_6N Isomers and Potential Energy Surface. ***C_4H_6N Isomers.*** Forty-five C_4H_6N isomers are identified in this work, as paraded in Figure 1 and s1 (Supporting Information)[41] the optimized structures for eight collision complexes and thirty-seven intermediates. Four isomers, **c1**, **c3**, **i3**, and **i6**, were predicted in the ab initio electronic structure calculations of Gannon et al. and employed in their master equations, which are essential but present a simpler picture of potential energy surface than ours. Specifically, only the paths of collision complexes **c1** and **c3** are included in their work, while in the present study, seven collision complexes are found probable.

Multireference Character. The T_1 diagnostics[43] (the Euclidian norm of $\mathbf{t}_1$ vector of the coupled cluster wave function) for the species in the reaction mechanisms in Figure 9 are listed in Table s5 (Supporting Information). For collision complexes **c1**−**c4**, and products, **p1**, **p2**, **p4**, and **p43**, the T_1's are less than 0.014, an indication that a single-reference wave function description is appropriate. It is perhaps not surprising that the transition states listed all have values larger than 0.02, sign of multireference nature.[43] With T_1's around 0.026, **c5**, **c7**, **c8**, and **i3** appear to have multireference character, however not substantial.

IV. Conclusion

The reaction of ground state cyano radical, $CN(X^2\Sigma^+)$, and propylene, $C_2H_3CH_3(X^1A')$, has been investigated by combining ab initio electronic structure calculations for predicting reaction paths, RRKM theory to yield rate constant for each path, and eventually solving rate equations for concentration evolutions and product ratios at zero pressure. Specifically, navigating via RRKM rate constants through the web of ab initio paths composed of eight collision complexes, 37 intermediates, 12 H-, 23 H_2-, 3 HCN-, and 4 CH_3-dissociation products, and the corresponding transition states, the most probable paths downsized to 7−9 species at collisions energies of 0 and 5 kcal/mol, respectively, are adopted as the reaction mechanisms. The rate equations for the reaction mechanisms are solved numerically such that the concentration evolutions are obtained.

This study predicts that the titled reaction via any of the seven collision complexes, **c1**−**c5, c7**, and **c8**, would generate products, **p1** + H, **p2** + H, and mostly **p43** (vinyl cyanide) + CH_3 for collision energy within 0−5 kcal/mol. As the H-dissociated **p1** and **p2** are exclusively stemming from the most stable collision complex **c1**, **p43** is produced by way of both **c1** (via **i3**) and **c3**. In addition to the insertion mechanism through collision complex, the direct H-abstraction of propylene by CN radical might occur and generate HCN + **p39**, HCN + **p40**. Propylene has been identified recently in the cold molecular cloud TMC-1,[44] and could play an important role in the chemistry of the interstellar medium. Our investigation indicates that the barrierless and exoergic $CN(X^2\Sigma^+) + C_2H_3CH_3(X^1A')$ reaction would be an efficient route for the **p1**, **p2**, **p43**, and likely **p39** and **p40** formation in cold molecular clouds and in the atmosphere of Saturn's satellite Titan.

Acknowledgment. Computer resources at the National Center for High-performance Computer of Taiwan were utilized in the calculations.

Supporting Information Available: Computed energies (Table s1), rate constants (Table s2), rate constants for the systems of CN + CD_3CHCH_2 (Table s3) and CN + CH_3CDCD_2 (Table s4), T_1 diagnostic (Table s5), optimized geometries for intermediates (Figure s1), products (Figure s2), and transition states (Figure s3), concentration evolutions at 0 and 5 kcal/mol (Figures s4 and s5), expanded mechanisms including **p4** (Figure s6), reaction paths (Figure s7) and mechanisms (Figure s8) for CN + CD_3CHCH_2 reaction, reaction paths (Figure s9) and mechanisms (Figure s10) for CN + CH_3CDCD_2 reaction. This material is available free of charge via the Internet at http://pubs.acs.org.

References and Notes

(1) Liang, M.; Yung, Y. L.; Shemansky, D. E. *Astrophys. J.* **2007**, *661*, L199.
(2) Coustenis, A.; Bézard, B.; Gautier, D.; Marten, A.; Samuelson, R. *Icarus* **1991**, *89*, 152.
(3) Coustenis, A.; et al. *Icarus* **2007**, *189*, 35.
(4) Hébrard, E.; Dobrijevic, M.; Bénilan, Y.; Raulin, F. *Planet. Space Sci.* **2007**, *55*, 1470.
(5) Raulin, F.; Coll, P.; Benilan, Y.; Bruston, P.; Gazeau, M.-C.; Paillous, P.; Smith, N.; Sternberg, R.; Coscia, D.; Israel, G. *Titan's chemistry: exobiological aspects and expected contribution from Cassini-Huygens. Exobiology: Matter Energy, and Information in the Origin and Evolution of Life in the Universe* **1998**, 301.
(6) Owen, T. C. *Planet. Space Sci.* **2000**, *48*, 747.
(7) Coustenis, A.; Taylor, F. *Titan - The Earth-Like Moon*; World Scientific: Singapore; 1999.
(8) Rodriguez, S.; Paillou, P.; Dobrijevic, M.; Ruffié, G.; Coll, P.; Bernard, J. M.; Encrenaz, P. *Icarus* **2003**, *164*, 213.
(9) McKay, C. P.; Coustenis, A.; Samuelson, R. E.; Lemmon, M. T.; Lorenz, R. D.; Cabane, M.; Rannou, P.; Drossart, P. *Planet. Space Sci.* **2000**, *49*, 79.
(10) Coll, P.; Coscia, D.; Smith, N.; Gazeau, M. C.; Ramirez, S. I.; Cernogora, G.; Israel, G.; Raulin, F. *Planet. Space Sci.* **1999**, *47*, 1331.
(11) Griffith, C. A.; Owen, T.; Miller, G. A.; Geballe, T. *Nature* **1998**, *395*, 575.
(12) Jiang, X.; Camp, C. D.; Shia, R.; Noone, D.; Walker, C.; Yung, Y. L. *J. Geophys. Res.-Atmos.* **2004**, 109 (D16).
(13) Roe, H. G.; Bouchez, A. H.; Trujillo, C. A.; Schaller, E. L.; Brown, M. E. *ApJ.* **2005**, *618*, L49.
(14) Lebonnis, S.; Toublanc, D.; Hourdin, F.; Rannou, P. *Icarus* **2001**, *152*, 384. Roe, H. G.; de Pater, I.; McKay, C. P. *Icarus* **2004**, *169*, 440.
(15) Griffith, C. A.; Owen, T.; Miller, G. A.; Geballe, T. *Nature* **1998**, *395*, 575.
(16) Sarker, N.; Somogyi, A.; Lunine, J. I.; Smith, M. A. *Astrobiology* **2003**, *3*, 719.
(17) Kerr, R. A. *Science* **2005**, *307*, 330. Wilson, E. *Chem. Eng. News* **2005**, *83*, 7. Wilson, E. *Chem. Eng. News* **2005**, *83*, 6. Wilson, E. *Chem. Eng. News* **2005**, *83*, 7.
(18) Jackson, W. M.; Scodinu, A. *Astrophysics and Space Science Library: The New Rosetta Targets. Observations, Simulations and Instrument Performances*; 2004; Vol. 311, p 85. Apaydin, G.; Fink, W. H.; Jackson, W. M. *J. Chem. Phys.* **2004**, *121*, 9368. Smith, N. S.; Raulin, F. *J. Geophys. Res.* **1999**, *104*, 1873.
(19) Smith, N. S.; Benilan, Y.; Bruston, P. *Planet. Space Sci.* **1998**, *46*, 1215.
(20) Wang, J. H.; Liu, K.; Min, Z.; Su, H.; Bersohn, R.; Preses, J.; Larese, J. Z. *J. Chem. Phys.* **2000**, *113*, 4146.
(21) Cody, R. J.; Romani, P. N.; Nesbitt, F. L.; Iannone, M. A.; Tardy, D. C.; Stief, L. J. *J. Geophys. Res.* **2003**, *108*, 5119. Cody, R. J.; Payne, W. A., Jr.; Thorn, R. P., Jr.; Nesbitt, F. L.; Iannone, M. A.; Tardy, D. C.; Stief, L. J. *J. Phys. Chem. A* **2002**, *106*, 606. Smith, G. P. *Chem. Phys. Lett.* **2003**, *376*, 381. (c) Davis, M. J.; Klippenstein, S. J. *J. Phys. Chem. A* **2002**, *106*, 5860.
(22) Seki, K.; Okabe, H. *J. Phys. Chem.* **1993**, *97*, 5284. Balko, B. A.; Zhang, J.; Lee, Y. T. *J. Chem. Phys.* **1991**, *94*, 7958. Läuter, A.; Lee, K. S.; Jung, K. H.; Vatsa, R. K.; Mittal, J. P.; Volpp, H.-R. *Chem. Phys. Lett.* **2002**, *358*, 314. Wodtke, A. M.; Lee, Y. T. *J. Phys. Chem.* **1985**, *989*, 4744. Segall, J.; Wen, Y.; Lavi, R.; Singer, R.; Wittig, C. *J. Phys. Chem.* **1991**, *95*, 8078. Okabe, H. *J. Chem. Phys.* **1983**, *78*, 1312.
(23) Lee, S.-H.; Lee, Y. T.; Yang, X. *J. Chem. Phys.* **2004**, *120*, 10983. Cromwell, E. F.; Stolow, A.; Vrakking, M. J. J.; Lee, Y. T. *J. Chem. Phys.*

1992, *97*, 4029. Balko, B. A.; Zhang, J.; Lee, Y. T. *J. Chem. Phys.* **1992**, *97*, 935. Chang, A. H. H.; Mebel, A. M.; Yang, X.-M.; Lin, S. H.; Lee, Y. T. *Chem. Phys. Lett.* **1998**, *287*, 301. Lin, J. J.; Hwang, D. W.; Lee, Y. T.; Yang, X. *J. Chem. Phys.* **1998**, *109*, 2979. Peña-Gallergo, A.; Martínez-Núñez, E.; Vázquez, S. A. *Chem. Phys. Lett.* **2002**, *353*, 418.

(24) Kaiser, R. I.; Balucani, N. *Acc. Chem. Res.* **2001**, *34*, 699.

(25) Huang, L. C. L.; Asvany, O.; Chang, A, H. H.; Balucani, N.; Lin, S. H.; Lee, Y. T.; Kaiser, R. I. *J. Chem. Phys.* **2000**, *113*, 8656.

(26) Balucani, N.; Asvany, O.; Chang, A. H. H.; Lin, S. H.; Lee, Y. T.; Kaiser, R. I.; Osamura, Y. *J. Chem. Phys.* **2000**, *113*, 8643.

(27) Balucani, N.; Asvany, O.; Chang, A. H. H.; Lin, S. H.; Lee, Y. T.; Kaiser, R. I.; Bettinger, H. F.; Schleyer, P. v. R.; Schaefer, H. F., III. *J. Chem. Phys.* **1999**, *111*, 7457.

(28) Balucani, N.; Asvany, O.; Kaiser, R. I.; Osamura, Y. *J. Phys. Chem. A* **2002**, *106*, 4301.

(29) Huang, L. C. L.; Balucani, N.; Lee, Y. T.; Kaiser, R. I.; Osamura, Y. *J. Chem. Phys.* **1999**, *111*, 2857.

(30) Gu, X. B.; Zhang, F. T.; Kaiser, R. I. *J. Phys. Chem. A* **2008**, *112*, 9607.

(31) Carty, D.; Page, V. L.; Sims, I. R.; Smith, I. W. M. *Chem. Phys. Lett.* **2001**, *344*, 310. Hoobler, R. J.; Leone, S. R. *J. Phys. Chem. A* **1999**, *103*, 1342.

(32) Smith, I. W. M.; Sage, A. M.; Donahue, N. M.; Herbst, E.; Quan, D. *Faraday Discuss.* **2006**, *133*, 137.

(33) Gannon, K. L.; Glowacki, D. R.; Blitz, M. A.; Hughes, K. J.; Pilling, M. J.; Seakins, P. W. *J. Phys. Chem. A* **2007**, *111*, 6679.

(34) Trevitt, A. J.; Goulay, F.; Meloni, G.; Osborn, D. L.; Taatjes, C. A.; Leone, S. R. *Int. J. Mass Spectrom.* **2009**, *280*, 113.

(35) (a) Becke, A. D. *J. Chem. Phys.* **1993**, *98*, 5648–5652. (b) 1992, *96*, 2155;(c) 1992, *97*, 9173. (d) Lee, C.; Yang, W.; Parr, R. G. *Phys. Rev. B* **1988**, *37*, 785.

(36) (a) Purvis, G. D.; Bartlett, R. J. *J. Chem. Phys.* **1982**, *76*, 1910. (b) Hampel, C.; Peterson, K. A.; Werner, H.-J. *Chem. Phys. Lett.* **1992**, *190*, 1. (c) Knowles, P. J.; Hampel, C.; Werner, H.-J. *J. Chem. Phys.* **1993**, *99*, 5219. (d) M. J. O. Deegan, M. J. O.; Knowles, P. J. *Chem. Phys. Lett.* **1994**, *227*, 321.

(37) (a) Mebel, A. M.; Morokuma, K.; Lin, M. C. *J. Chem. Phys.* **1995**, *107*, 7414. (b) Bauschlicher, C. W., Jr.; Partridge, H. *Chem. Phys. Lett.* **1995**, *240*, 533. (c) Bauschlicher, C. W., Jr.; Partridge, H. *J. Chem. Phys.* **1995**, *103*, 1788.

(38) Frisch, M. J. et al., *GAUSSIAN 98*, revision A.5; Gaussian, Inc.: Pittsburgh, PA, 1998. Frisch, M. J.; et al. *GAUSSIAN 03*, revision C.02; Gaussian, Inc.: Wallingford CT, 2004.

(39) Eyring, H.; Lin, S. H.; Lin, S. M. *Basic Chemical Kinetics*; Wiley: New York, 1980.

(40) Chang, A. H. H.; Mebel, A. M.; Yang, X. M.; Lin, S. H.; Lee, Y. T. *J. Chem. Phys.* **1998**, *109*, 2748.

(41) Supporting Information.

(42) Vereecken, L.; Groof, P. D.; Peeters, J. *Phys. Chem. Chem. Phys.* **2003**, *5*, 5070.

(43) Lee, T.; Taylor, P. R. *Int. J. Quant. Chem. Sym.* **1989**, *23*, 199.

(44) Marcelino, N.; Cernicharo, J.; Agundez, M.; Roueff, E.; Gerin, M.; Martin-Pintado, J.; Mauersberger, R.; Thum, C. *ApJ*. **2007**, *665*, L127.

JP905081U